Photochemical & Photobiological Sciences

RSC Publishing

PAPER

View Article Online
View Journal | View Issue

Photochemistry of aqueous solutions of kynurenic acid and kynurenine yellow†

Cite this: *Photochem. Photobiol. Sci.*, 2013, **12**, 546

Ekaterina A. Zelentsova,[a,b] Peter S. Sherin,[a,c] Olga A. Snytnikova,[a,b] Robert Kaptein,[b,d] Eric Vauthey[c] and Yuri P. Tsentalovich*[a,b]

Received 25th October 2012,
Accepted 2nd December 2012

DOI: 10.1039/c2pp25357g

www.rsc.org/pps

The photophysics and photochemistry of kynurenic acid (KNA) and kynurenine yellow (KNY) in neutral aqueous solutions were investigated using time-resolved optical spectroscopy. Both molecules have similar quinoline-like structures, the only difference being the absence of conjugation in the nitrogen containing cycle in KNY. The main channel of S_1 excited state decay in the case of partially-unconjugated KNY is the solvent assisted $S_1 \rightarrow S_0$ radiationless transition *via* intermolecular hydrogen bonds ($\Phi_{IC} = 0.96$), whereas, in the case of fully-conjugated KNA, it is intersystem crossing to the triplet state ($\Phi_T = 0.82$). The major intermediate products of the singlet excited KNY deactivation are the triplet state ($\Phi_T = 0.022$) and, most probably, the enol form ($\Phi_{enol} = 0.012$), which decay with the formation of 2,3-dihydro-4-hydroxyquinoline and 4-hydroxyquinoline, respectively. The results obtained show that KNA and KNY, which are products of the decomposition of the UV filter kynurenine, are significantly more photoactive and less photostable than the parent molecule.

Introduction

Photoprotection of the human eye is provided by molecular UV filters, consisting of low molecular weight compounds contained in the lens and absorbing UV light in the 300–400 nm spectral region. The main deactivation pathway of the photoexcited UV filter in aqueous solutions is solvent-assisted internal conversion to the ground state, which proceeds with an efficiency of about 99%.[1,2] The "primary" UV filters, namely kynurenine (KN), 3-hydroxykynurenine (3OHKN) and 3-hydroxykynurenine *O*-β-D-glucoside (3OHKG), are synthesized enzymatically from tryptophan.[3–6] Under physiological conditions, these compounds can undergo spontaneous deamination[7,8] yielding highly reactive carboxyketoalkenes (CKAs), the subsequent reactions of the latter resulting in the production of "secondary" UV filters, *e.g.* glutathionyl-3-hydroxykynurenine glucoside, 4-(2-amino-3-hydroxyphenyl)-4-oxobutanoic acid *O*-β-D-glucoside, and 4-(2-amino-3-hydroxyphenyl)-4-oxobutanoic acid *O*-β-D-diglucoside.[7,9,10] All these compounds are present in the human lens at concentrations varying from about 500 nmoles g^{-1} (3OHKG, young lenses) to 1–2 nmoles g^{-1} (3OHKN, old lenses).[11]

The decomposition of UV filters gives rise to the formation of different products. For example, the reactions of KN can result in the formation of 4-hydroxyquinoline (4HQN),[8] xanthurenic acid (XAN),[12,13] kynurenine yellow (KNY),[7] and kynurenic acid (KNA).[14,15] However, the concentrations of these products in the human lens are either much smaller than that of the UV filters, or below the limit of detection. That may indicate that these products are chemically or photochemically much more active than the original UV filters, and, once produced, undergo chemical reactions, so their abundance in the lens remains very low. The reactions of the products of UV filter decomposition may cause post-translational modifications of the lens proteins and promote the development of cataract. Thus, the investigation of the reactivity of these compounds is important for a better understanding of the role of UV-induced processes in the mechanisms of cataractogenesis.

In our previous work, we studied the properties of the ground and photoexcited states of 4HQN and XAN.[16,17] These investigations have revealed that both compounds are much better photosensitizers than UV filters: the major short-lived intermediates formed under UV irradiation in neutral aqueous solution being a triplet state in the case of 4HQN, and an enol form for XAN. This paper is devoted to the investigation of the photophysics and photochemistry of KNA and KNY in aqueous solutions, the chemical structures of these molecules being shown in Chart 1. KNY is the major product of KN thermal

[a]*International Tomography Center SB RAS, Institutskaya str., 3A, 630090 Novosibirsk, Russia*
[b]*Novosibirsk State University, Pirogova str. 2, 630090 Novosibirsk, Russia. E-mail: yura@tomo.nsc.ru; Fax: +7-383-3331399; Tel: +7-383-3303136*
[c]*Department of Physical Chemistry, University of Geneva, quai Ernest-Ansermet 30, CH-1211 Geneva, Switzerland*
[d]*Bijvoet Center, Utrecht University, Utrecht, The Netherlands*
†Electronic supplementary information (ESI) available. See DOI: 10.1039/c2pp25357g

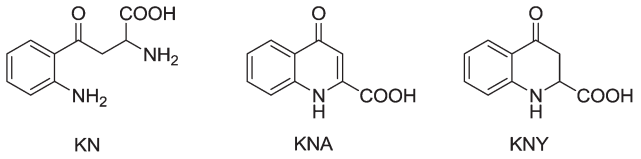

Chart 1

decomposition, formed in the cyclization reaction of CKA;[7,18] however, up to date, the presence of KNY in mammalian lenses has not been reported. To the best of our knowledge, the photochemical properties of this compound have not been studied.

KNA can be synthesized from KN either enzymatically,[15,19,20] or through an oxidative pathway.[14] It was found in various human tissues;[15,21,22] in a normal human lens, the KNA level is about 1 nmole g^{-1}, whereas in a cataractous lens, this level increases markedly.[23] The elevation of the KNA level has been also revealed in the cataractous lenses of rats.[24] In a study of the spectroscopic and photosensitizing properties of KNA by Pileni *et al.*,[25,26] it had been shown that the photolysis of KNA results in population of its triplet state, the latter being able to oxidize amino acids and other substrates. The photosensitizing properties of KNA were confirmed by the work of Krishna *et al.*,[27] which reported a significant singlet oxygen yield upon UV irradiation of KNA solutions. Conversely, the ability of KNA to scavenge free radicals and to reduce reactive oxygen species formation has been reported.[28] Thus, the data on the oxidative properties of KNA found in the literature seem to be somewhat contradictive, and the mechanism of KNA photolysis requires a more detailed quantitative analysis.

Experimental part

Materials

D,L-Kynurenine, kynurenic acid and quinine bisulphate were from Sigma/Aldrich, 2-aminopyridine from Acros, acetonitrile HPLC grade from Panreac, deuterated water from Armar and were used as received. H_2O was distilled and deionized (18 MΩ).

Kynurenine yellow (KNY) was synthesized as follows: an aqueous solution of KN (7 mM, pH 9) was de-aerated with argon, then capped, sealed with parafilm and incubated in a thermostat at 70 °C for 24 hours. After incubation and filtration, the solution was separated by HPLC (LC 1200, Agilent) equipped with a multiple wavelength UV-Vis detector on a C16 preparative column (16 × 250 mm, 7 μm, Diasorb-130-C16-T; BioChimMac ST, Russia). Separation was performed using an acetonitrile/0.05% (v/v) TFA in H_2O gradient. The acetonitrile percentage in the gradient was 0% (0–3 min), 0–30% (3–5 min), 30–45% (5–35 min), 45–100% (35–37 min), 100% (37–38 min), 100–0% (38–40 min), 0% (40–45 min). The flow rate was 4 mL min^{-1}, the injection volume was 1 mL, and the detection was performed simultaneously at five wavelengths – 280, 320, 360, 380 and 400 nm. The fraction containing KNY (retention time 18.3 min) was collected, lyophilized, and stored at −20 °C until use. The identity of KNY was verified by mass-spectrometry using an Esquire6000 (Bruker Daltonics) ion trap and by NMR spectrometry with an Avance 400 (Bruker Spectrospin) NMR spectrometer. The ions detected in MS measurements (positive mode) are: molecular ion m/z 192, fragments m/z 174 (H_2O loss), m/z 164 (CO loss), m/z 146 (CO + H_2O loss). ^1H NMR data (400 MHz, D_2O): aliphatic: δ = 3.07 (m, 2 H, CH_2), δ = 4.46 (dd, J = 7.3 Hz, J = 6.0 Hz, 1 H, CH); aromatic: δ = 6.88 (t, J = 8.0 Hz, 1 H), δ = 6.99 (d, J = 8.1 Hz, 1 H), δ = 7.52 (td, J = 7.8 Hz, J = 1.6 Hz, 1 H), δ = 7.76 (dd, J = 8.0 Hz, J = 1.6 Hz, 1 H).

Steady-state optical measurements

UV-visible electronic absorption spectra were recorded with an Agilent 8453 (Hewlett–Packard) and a Cary 50 (Varian) spectrophotometer. Fluorescence and emission spectra were measured with a FLSP920 (Edinburgh Instruments) spectrofluorimeter. The fluorescence quantum yields of KNA and KNY were determined relatively to a 0.1 N H_2SO_4 aqueous solution of 2-aminopyridine (λ_{ex} = 315 nm, Φ_F = 0.60)[29] and to a 1 N H_2SO_4 aqueous solution of quinine bisulphate (λ_{ex} = 366 nm, Φ_F = 0.56),[30] respectively. All fluorescence spectra were corrected for the wavelength-dependent sensitivity of the detection. For all measurements, a 10 × 10 mm^2 quartz cell was used, and the absorbance of samples was below 0.1 at the absorption maximum.

Steady-state photolysis

The solutions for steady-state photolysis were prepared in a phosphate buffer (pH 6.8), the sample concentrations (around 1 mM) were adjusted in such a way that all solutions had the same absorbance of A = 3.0 at the absorption maxima for a 1 cm optical path. The samples were placed in NMR glass tubes (5 mm outer diameter) and irradiated with a DRSh-1000 mercury lamp. The sample volume was 1 cm^3. A water filter was used to cut off infrared light, and the 300–400 nm region was selected with a set of UV glass filters. The solutions were bubbled with argon or oxygen for 10 min prior to and during irradiation. During photolysis, samples (15 μL) were periodically taken off with a syringe and stored at 4 °C until use. These samples were diluted with water up to 200 μL and analyzed by HPLC.

Actinometry was performed using an aqueous solution of potassium ferri-oxalate according to standard methods.[31] The intensity of light on the sample in the 300–400 nm region was equal to $(1.1 \pm 0.1) \times 10^{18}$ quanta per second.

The HPLC analysis of the irradiated samples was performed on a 4.6 × 150 mm, 5 μm, ZORBAX Eclipse XBD-C18 analytical column using an acetonitrile/0.05% (v/v) TFA in H_2O gradient. The acetonitrile percentage in the gradient was 0% (0–5 min), 0–20% (5–5.1 min), 20–80% (5.1–25 min), 80–100% (25–26 min), 100% (26–30 min), 100–0% (30–31 min), 0% (31–45 min). The flow rate was 1 mL min^{-1}, the samples (volume 50 μL) were injected with the use of an autosampler thermostated at 4 °C, and the detection was performed

simultaneously at four wavelengths – 320, 332, 360 and 380 nm. The chromatograms were recorded and the peak areas integrated using Agilent ChemStation for Windows.

Time-resolved fluorescence measurements

The early fluorescence dynamics was recorded using a fluorescence up-conversion setup described in detail elsewhere.[32] Briefly, a part of the output of a tunable mode-locked Ti:sapphire laser (Spectra Physics "MaiTai") was frequency-doubled and used to excite the sample at 400 nm. The polarization of the probe pulses was at the magic angle relative to that of the gate pulses at 800 nm. The fluorescence was gated by sum-frequency mixing with the fundamental of the oscillator output. The up-converted UV photons were directed into a monochromator and detected by a photomultiplier tube with photon counting electronics. The sample solutions were kept in a 1.0 mm thick spinning cell and had an absorbance of about 0.2 at the excitation wavelength. The full width at half-maximum (FWHM) of the instrument response function was around 210 fs.

The fluorescence dynamics on the nanosecond time scale was detected using a time-correlated single photon counting (TCSPC) unit of a FLSP920 spectrofluorimeter (Edinburgh Instruments). A pulsed light emitting diode (EPLED-330, λ = 330 nm, FWHM ≈ 800 ps) was used for the irradiation of KNA samples, and a pulsed diode laser (EPL-375, λ = 375 nm, FWHM ≈ 80 ps) – for the irradiation of KNY samples. The time profiles were recorded at the maxima of fluorescence bands with a 50 MHz repetition rate. A 10 × 10 mm^2 quartz cell was used; the sample absorbance at the absorption maximum was below 0.1. The fluorescence time profiles obtained were analyzed using the convolution of the experimental instrument response function with either an exponential function or a sum of two exponential functions.

Transient absorption (TA) measurements

The TA dynamics at femtosecond time scale was carried out with the experimental setup described in ref. 33, 34. Excitation was performed at 400 nm using the frequency doubled output of a standard 1 kHz amplified Ti : Sapphire system (Spectra-Physics). The pump intensity on the sample was around 1.5 mJ cm^{-2}. Probing was achieved with a white-light continuum obtained by focusing a small fraction of the 800 nm pulses in a CaF_2 plane window. The polarization of the probe pulses was at the magic angle relative to that of the pump pulses. All spectra were corrected for the chirp of the white light probe pulses. The FWHM of the instrument response function was *ca.* 200 fs. The sample solutions were placed in a 1 mm thick quartz cell where they were continuously stirred by N_2-bubbling. Their absorbance at the excitation wavelength was around 0.2.

Slower TA dynamics was recorded with a nanosecond laser flash photolysis (LFP) setup described earlier.[35] Briefly, solutions, placed in a rectangular cell (inner dimensions 10 mm × 10 mm), were irradiated with either a Quanta-Ray LAB-130-10 Nd : YAG laser (355 nm, pulse duration 8 ns, pulse energy up to 135 mJ), or a Lambda Physik EMG 101 excimer laser (308 nm, pulse duration 15–20 ns, pulse energy up to 100 mJ). A fraction of the laser beam was split by a quartz plate and directed to a photodiode for triggering the oscilloscope and to a Newport 1918-C power meter for the permanent monitoring of the laser energy. The dimensions of the laser beam at the front of the cell were 2.5 mm × 8 mm. The monitoring system includes a DKSh-150 xenon short-arc lamp connected to a high current pulser, a Newport 78025 monochromator, a 9794B photomultiplier (Electron Tubes Ltd.), and a LeCroy WaveRunner 104MXi digital oscilloscope. The monitoring light, concentrated in a rectangle of 2.5 mm height and 1 mm width, passed through the cell along the front (laser irradiated) window. Thus, in all experiments the excitation optical length was 1 mm, and the monitoring optical length was 8 mm. All solutions were bubbled with argon or oxygen for 10 minutes prior to and during irradiation.

Results

1. Steady-state measurements

1.1. Steady-state absorption spectra. The electronic absorption spectrum of KNA in neutral aqueous solution exhibits a band with a maximum at 332 nm and shoulders at 320 nm and 345 nm (Fig. 1A). The shape of the spectrum significantly changes in acidic and basic solutions (ESI, Fig. S1†). A titration curve of the absorbance at 345 nm, where the spectral changes are the most pronounced, was measured (ESI, inset of Fig. S1†). The obtained pK_{a1} = 2.5 and pK_{a2} = 11.6 values are in good agreement with a previous report.[25] Since the dissolution of KNA in neutral water leads to the acidification of solution, one can conclude that under physiological conditions KNA is present in the anionic form. Thus, the value pK_{a1} can be attributed to the protonation of either an acidic group with the formation of a neutral molecule, or an amino

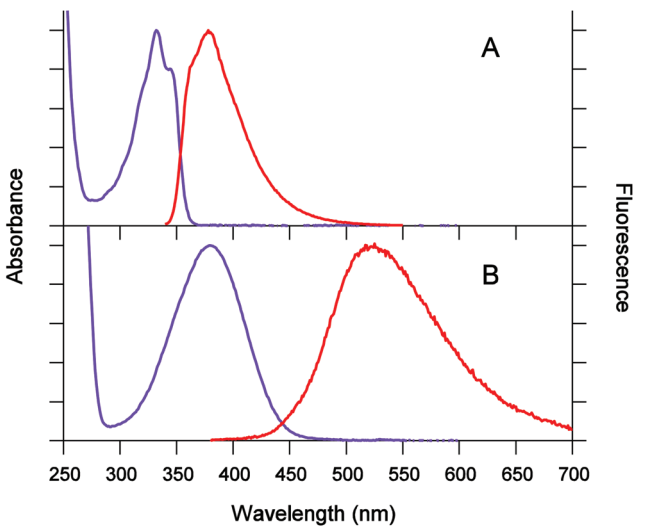

Fig. 1 Absorption (blue traces) and fluorescence (red traces) spectra of (A) KNA and (B) KNY in neutral aqueous solution.

group to give a zwitterionic form. Quantum chemical calculations[17] for a similar compound, xanthurenic acid, demonstrated that the neutral and zwitterionic forms have almost equal Gibbs free energies, so it is difficult to predict which form of KNA is preferable at low pH. The second titration point pK_{a2} should be attributed to the deprotonation of the amino group.

The absorption spectrum of KNY in neutral aqueous solution is characterized by bands with maxima at 235 nm, 260 nm (not shown) and 380 nm (Fig. 1B), similarly to those of KN[36] and other UV filters contained in the human eye.[2,35] Measurements at different pH values showed only one protonation site (COO– group), which has a very weak conjugation with the chromophore part of the molecule. In acidic solution, the absorption band undergoes a slight shift from 380 nm to 373 nm, whereas no changes were observed in basic solutions (ESI, Fig. S2†). Titration of KNY performed by monitoring the absorbance at 400 nm (ESI, inset of Fig. S2†) yielded a dissociation constant of pK_a = 3.7. The difference of pK_a values between the COO– groups of KNA and KNY should be attributed to a stronger conjugation of this group with the aromatic part of the molecule in KNA.

1.2. Steady-state fluorescence spectra. The fluorescence emission spectra of KNA and KNY in neutral aqueous solution are shown in Fig. 1. For both compounds, the fluorescence excitation spectra practically coincide with the absorption spectra, and the fluorescence emission spectra do not depend on the excitation wavelength (ESI, Fig. S3†). These observations testify that, in neutral aqueous solutions, both KNA and KNY are present in a single tautomeric form. The fluorescence spectrum of KNA is similar to that of 4HQN,[16] which exists only in the keto form in neutral aqueous solution.[16,37] Since the chemical structures of 4HQN and KNA are similar, one can presume that the keto form is the major tautomeric state of KNA in neutral aqueous solution as well. NMR data on KNY (see Materials) testify that in neutral solution KNY is also present in the keto form. The measured fluorescence quantum yields are $\Phi_F = (1.4 \pm 0.2) \times 10^{-3}$ for KNA and $\Phi_F = (7.5 \pm 1.0) \times 10^{-3}$ for KNY.

1.3. Steady-state photolysis. The photolysis of KNA and KNY was performed in aqueous neutral solutions under both aerobic and anaerobic conditions. Since the decomposition of KNY proceeded much faster than that of KNA, the irradiation of KNY was performed with a 5% neutral density filter. Fig. 2 shows the kinetics of the starting material decomposition under steady-state UV irradiation. Both compounds exhibit faster decomposition under anaerobic conditions as compared with aerobic ones, the difference between anaerobic/aerobic conditions being more pronounced with KNY. The quantum yields of photodecomposition were calculated using the part of the time profile where the compound concentration decreases almost linearly. The obtained values for KNA are Φ_{dec}(KNA, Ar) = $(6.0 \pm 1.5) \times 10^{-3}$, Φ_{dec}(KNA, O_2) = $(2.6 \pm 0.6) \times 10^{-3}$ and for KNY – Φ_{dec}(KNY, Ar) = $(3.0 \pm 0.8) \times 10^{-2}$, Φ_{dec}(KNY, O_2) = $(8 \pm 2) \times 10^{-3}$. The same tendency of a decreased decomposition rate in the presence of oxygen has been observed for KNA in the work of Pileni *et al.*,[26] although the decomposition yields measured here are somewhat higher than those reported in ref. 26. This observation testifies that the quenching of KNA and KNY excited states by oxygen reduces product formation.

HPLC analysis of KNA irradiated samples revealed numerous photodecomposition products, the identification of which has not been performed. In the case of KNY, the formation of two major products has been observed. Fig. 3 displays an example of a HPLC chromatogram obtained during the analysis of an irradiated KNY sample in buffered solution at pH 7.4. The first signal with a retention time of 9.8 min co-eluted with the standard 4HQN has the same UV-Vis spectrum, and displays a molecular ion with m/z = 146 and a fragment with m/z = 128 (H_2O loss). The peak at 11.4 min with an absorption spectrum similar to that of KNY and a molecular ion with m/z = 148, and fragments with m/z = 130 (H_2O loss) and m/z = 120 (CO loss) was attributed to 2,3-dihydro-4-hydroxyquinoline (DHQN). The open and solid triangles in Fig. 2B show the time

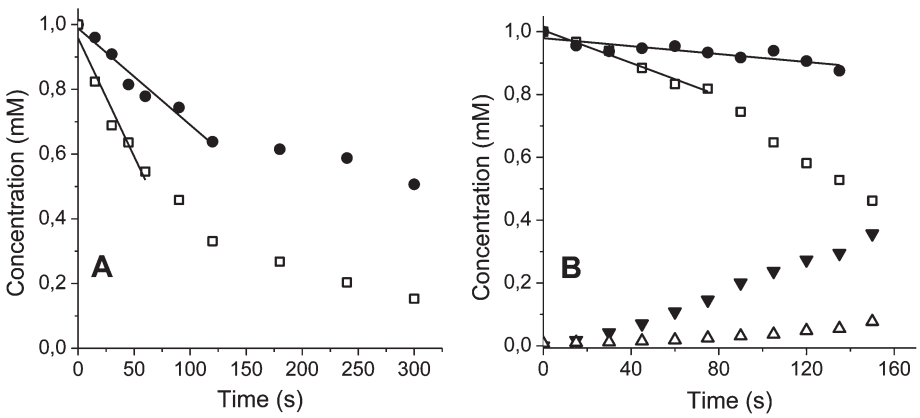

Fig. 2 Kinetics of anaerobic (squares) and aerobic (circles) photodecomposition of (A) KNA and (B) KNY in aqueous buffered solutions, pH 7.4. The open and solid triangles show the kinetics of the formation of 4HQN and DHQN, respectively. The data were obtained from the integration of HPLC profiles of the irradiated samples. Solid lines show linear fits.

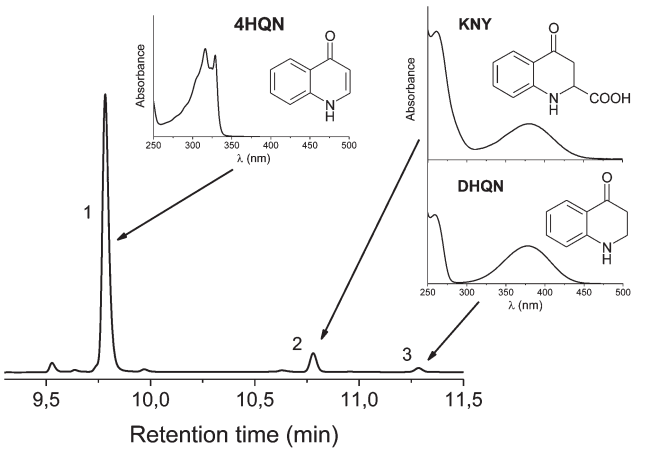

Fig. 3 HPLC profile of the irradiated sample of KNY in aqueous buffered solution, pH 7.4, detection at 320 nm. The peaks were identified as follows: 1. 4HQN (9.8 min), 2. KNY (10.8 min), 3. DHQN (11.4 min).

profiles of 4HQN and DHQN formation under anaerobic conditions. The calculated quantum yields of 4HQN and DHQN formation are $\Phi_{4HQN} = (1.2 \pm 0.4) \times 10^{-2}$ and $\Phi_{DHQN} = (2.2 \pm 0.6) \times 10^{-2}$. The sum of Φ_{4HQN} and Φ_{DHQN} is close to the Φ_{dec}(KNY, Ar) value, which testifies that 4HQN and DHQN are the main products of KNY anaerobic photolysis. It is important to note that the presence of oxygen blocks the formation of DHQN almost completely, whereas the formation of 4HQN under aerobic conditions is practically the same as in argon-saturated solutions.

2. Time-resolved measurements

2.1. Femtosecond fluorescence measurements. The fluorescence dynamics of KNY in H_2O at pH 6.7 upon 400 nm excitation was measured at 9 wavelengths throughout the emission band over different time windows up to 400 ps. The intensity-normalized time profiles are shown in Fig. 4A, and the early dynamics at the same wavelengths is displayed in Fig. 4B. The fast decay of the intensity at short wavelengths and the corresponding rise at long wavelengths are characteristic features of solvent relaxation leading to a red shift of the emission spectrum, a so-called dynamic Stokes shift. This shift can be clearly seen in Fig. 4C, where the reconstructed time-resolved emission spectra are presented. After this dynamic shift, the shape of the emission spectrum remains unchanged and coincides with the steady-state emission spectrum (grey line).

The obtained data were analyzed globally using a sum of exponential functions convolved with the Gaussian-like instrument response function. A good agreement between experimental and calculated data was achieved with four exponential functions, the best fits being shown in Fig. 4A and 4B and the corresponding time constants τ_i (i = 1,2,3,4) listed in Table 1. Fig. 4D shows the spectrum of each pre-exponential factor $A_i(\lambda)$, used in the global analysis, the so-called Decay Associated Spectra (DAS). Positive DAS amplitudes correspond to decay, and negative ones to a rise of signal intensity. The $A_1(\lambda)$ and $A_2(\lambda)$ spectra exhibit positive and negative bands, indicating a decay on the blue side and a rise on the red side of the emission band. These components can be attributed to the dynamic Stokes shift. The τ_3 DAS exhibits mostly positive values indicating a decay of the fluorescence signal with a minor negative contribution on the red side of the spectrum. The last DAS, associated with the largest time constant, almost coincides with the steady-state emission spectrum (thin grey line). Thus, τ_4 was attributed to the decay of the S_1 state of KNY. We should note that the accuracy on τ_4 in these measurements is rather low, as the obtained value varied significantly with the sample degradation. Because of this, the long-lived component was fitted globally, and only its average value over different wavelengths is presented in Table 1. This value should be considered as a rough estimate only. The fluorescence dynamics of KNA on a femtosecond timescale have not been studied because KNA does not absorb in the range of 370–520 nm available for excitation in our up-conversion setup.

2.2. Nanosecond fluorescence measurements. More accurate measurements of the S_1 state lifetime of KNY in aqueous solution were carried out by TCSPC, where much less excitation intensity is used compared to up-conversion. An example of the fluorescence time profile recorded with KNY in aqueous solution (pH 6.7, excitation at 375 nm, detection at 510 nm) is presented in ESI, Fig. S4.† The obtained kinetic curves were treated as a sum of two exponentials (with time constants τ_4 and τ_5, and relative amplitudes A_4 and A_5) numerically convolved with the instrument response function (IRF). The obtained results (τ_4 = 0.35 ns, A_4 = 0.994, τ_5 = 3.1 ns, A_5 = 0.006) show that, on a time scale longer than 100 ps, the fluorescence decay is almost purely mono-exponential with a lifetime of 350 ps. The minor component with the time constant τ_5 = 3.1 ns was attributed to a contribution from impurities present in solution. Similar fluorescence dynamics were observed with KNY in acidic (pH 1.3, τ_4 = 0.38 ns) and basic solutions (pH 13, τ_4 = 0.37 ns), indicating that the fluorescence lifetime of KNY is not pH dependent. Similarly, no dependence on the presence of buffer salts could be observed (Table 1). However, the τ_4 value increases almost twice to 620 ps in deuterated water pointing to a participation of intermolecular hydrogen bonding in the deactivation of the S_1 excited state of KNY.

TCSPC measurements were also performed with aqueous KNA solutions (pH 6.8, excitation at 330 nm, detection at 380 nm, ESI, Fig. S5†). The obtained fluorescence lifetime of τ_4 = 150 ps should be considered as an estimate only, since this value is at the limit of the temporal resolution of the TCSPC unit equipped with the 330 nm excitation source (EPLED330). The KNA fluorescence lifetime has been estimated earlier to be ≤200 ps using Br^- as a fluorescence quencher.[25] Measurements with KNA in aqueous solutions at various pH values and in heavy water revealed no effect of pH, presence of buffer, or isotopic effect (not shown). This observation testifies that intermolecular hydrogen bonds do not play a significant role in the decay of the S_1 state population of KNA.

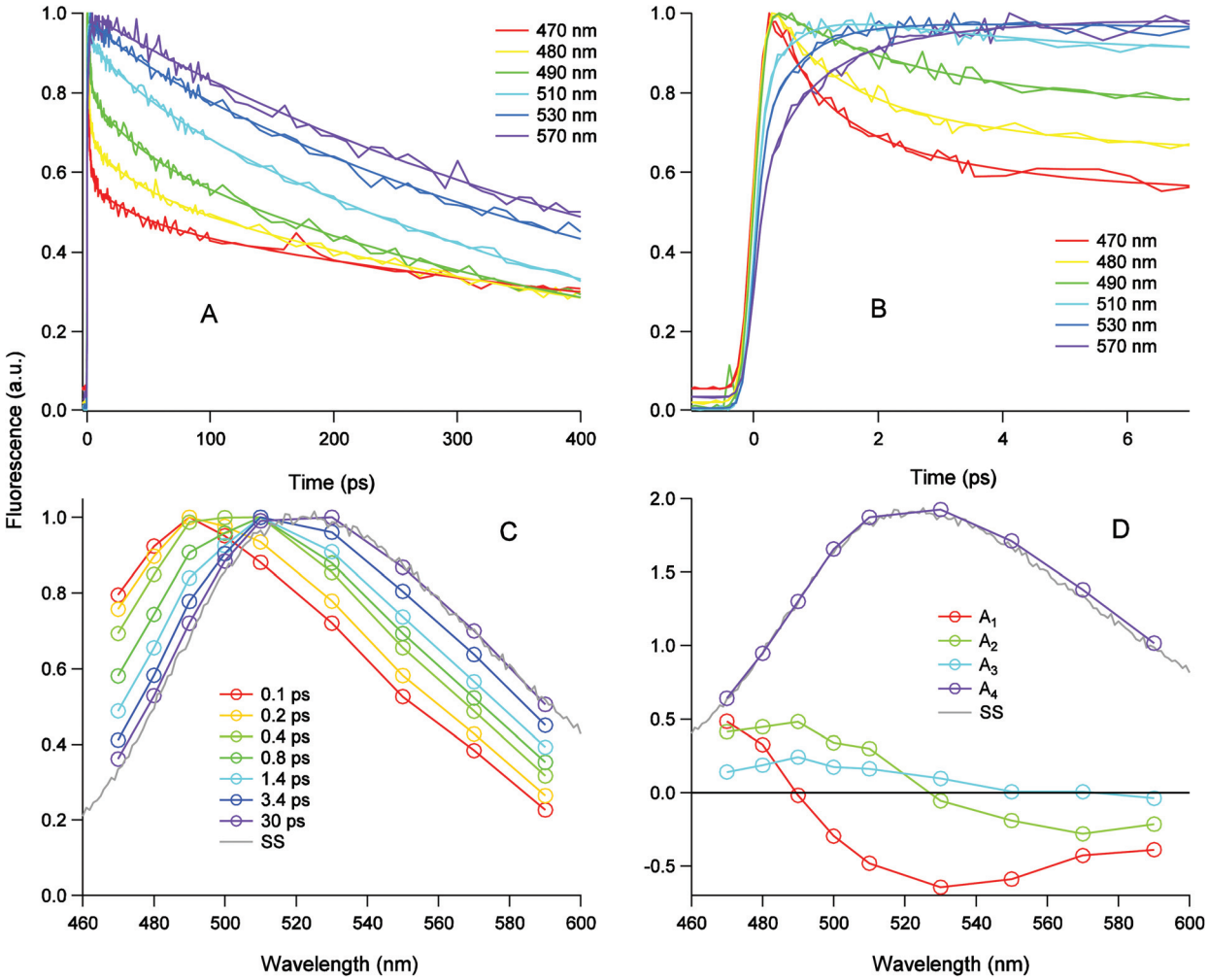

Fig. 4 (A) Fluorescence time profiles recorded with KNY in neutral aqueous solution, pH 6.7, after 400 nm excitation; the smooth lines represent the best 4-exponential fit. (B) Early dynamics at the same wavelengths. (C) Intensity-normalized time-resolved emission spectra. (D) DAS obtained from a global analysis of the fluorescence time profiles. The grey traces represent the steady-state fluorescence spectrum.

Table 1 Fluorescence quantum yields (Φ_F) and time constants (τ_i, i = 1, 2, 3, 4) obtained from a global analysis of the time-resolved fluorescence and TA data with KNY. The experimental errors for all listed values are 10%

Solution	Φ_F	τ_1/ps	τ_2/ps	τ_3/ps	τ_4/ps
Phosphate buffer saline, pH 7.4	0.0073	0.54[a]	1.9[a]	35[a]	370[a] 380[b]
H_2O pH 6.7	0.0075	0.53[a] 0.59[c]	1.8[a] 2.1[c]	32[a] 39[c]	360[a] 510[c] 350[b]
H_2O pH 1.3	0.0068	0.52[a]	2.0[a]	46[a]	370[a] 380[b]
H_2O pH 13	0.0072	0.58[a]	2.8[a]	31[a]	340[a] 370[b]
D_2O	0.012	0.60[a]	2.4[a]	39[a]	840[a] 620[b]

[a] TA data, λ_{ex} = 400 nm; [b] TCSPC data, λ_{ex} = 375 nm; [c] Up-conversion data, λ_{ex} = 400 nm.

2.3. Femtosecond TA measurements. Fig. 5A illustrates TA spectra recorded with KNY in H_2O at pH 6.9 at various time delays after 400 nm excitation. Immediately after excitation, a TA band with a maximum at 535 nm and shoulders at 460 and 650 nm is visible. During first 2 ps after excitation, the band maximum shifts from 535 to 525 nm, the dip at about 480 nm vanishes, and another dip appears around 600 nm. Within the following 35 ps, a growth of the TA signal in the 470–670 nm region can be observed. The subsequent dynamics exhibits a monotonic decay without significant spectral changes. The observed TA spectra consist of a superposition of $S_n \leftarrow S_1$ absorption (excited state absorption, ESA) and $S_1 \rightarrow S_0$ stimulated emission (SE) bands. Indeed, the fluorescence spectrum overlaps with the ESA band over almost the whole spectral window (see Fig. 1). Thus, the early dynamics could be assigned to the time-dependent Stokes shift of the $S_1 \rightarrow S_0$ SE band and, possibly, to a blue shift of the ESA band, due to the stabilization of the S_1 state upon solvation. The subsequent increase of the TA signal might originate from a partial decay of the SE, corresponding to the time constant τ_3 found in the fluorescence up-conversion measurements of KNY (see $A_3(\lambda)$,

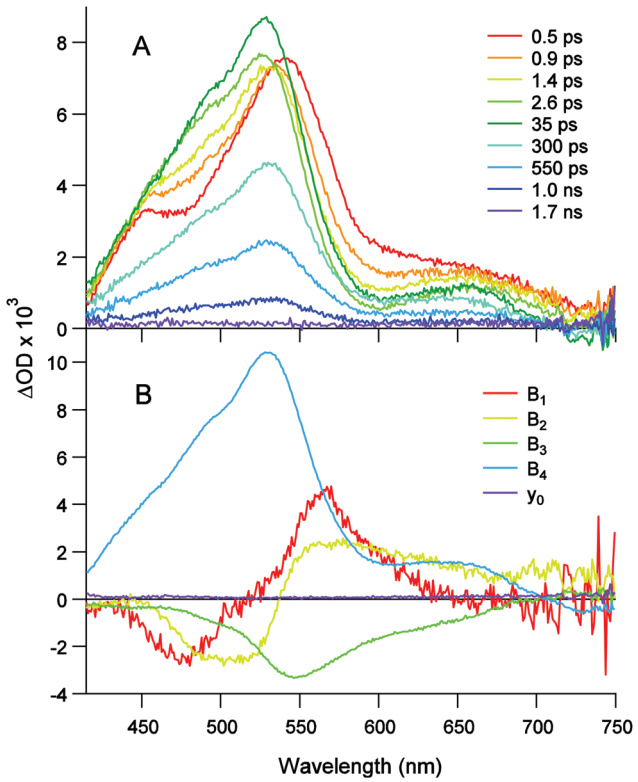

Fig. 5 (A) TA spectra at various time delays after 400 nm excitation of KNY in neutral aqueous solution, pH 6.9. (B) DAS obtained from a global analysis of TA data.

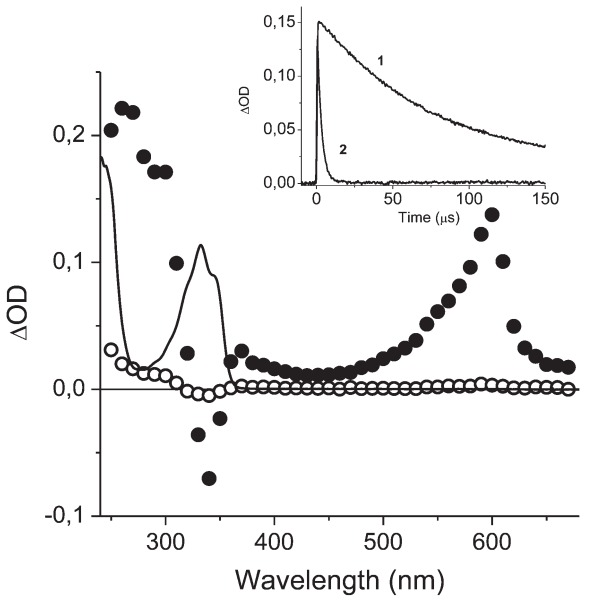

Fig. 6 TA spectra recorded with 1×10^{-4} M KNA in buffered aqueous solution, pH 7.2, 20 μs after 308 nm excitation under argon (solid circles) and oxygen (open circles). Solid trace: steady-state absorption spectrum of KNA. Inset: TA time profiles at 600 nm under argon (1) and oxygen (2).

Fig. 4D). The monotonic decay and the absence of any significant absorption after the decay of the main TA band indicate that the formation product does not make a significant contribution in the observed TA dynamics.

The TA data were analyzed globally using the sum of four exponential functions and time constants very similar to those obtained from the fluorescence up-conversion measurements. The resulting DAS $B_i(\lambda)$, i = 1,2,3,4 are shown in Fig. 5B (y_0 is the residual signal), and the corresponding time constants are listed in Table 1. The shapes of the DAS, related to the two fastest components, are similar to the DAS obtained in the fluorescence measurements (Fig. 4D), but have opposite signs because of the negative intensity of the SE band in the TA spectra. Therefore, these components can be assigned to the dynamic Stokes shift of the SE. The third DAS exhibits a broad negative band with a small positive tail at $\lambda > 700$ nm. We have presently no explanation for the origin of this time constant. The last DAS is related to a time constant close to the S_1 lifetime obtained in fluorescence experiments, and can thus be attributed to the decay of the S_1 state population.

2.4. Nanosecond laser flash photolysis measurements. Fig. 6 shows TA spectra obtained during 308 nm photolysis of 1×10^{-4} M KNA in buffered aqueous solution (pH 7.2) 20 μs after the laser flash under anaerobic (solid circles) and aerobic (open circles) conditions. The transient with the absorption maxima around 260 nm and 600 nm is readily quenched by oxygen (see the inset of Fig. 6 for the kinetic curves) with a rate constant of 2.9×10^9 M^{-1} s^{-1} that allows an assignment of this signal to the KNA triplet state. Under anaerobic conditions, the signal decays by second-order kinetics with $k_2/\varepsilon = 4.6 \times 10^5$ cm s^{-1} for 600 nm and $k_2/\varepsilon = 2.7 \times 10^5$ cm s^{-1} for 290 nm, and no formation of other intermediates or products has been observed. This testifies that, in the absence of quenchers, the major triplet decay channel is triplet–triplet annihilation. The same triplet state behavior has been observed for the related compound 4HQN.[16]

The kinetics observed under 355 nm photolysis of KNY buffered aqueous solution (2.4×10^{-4} M, pH 7.2) is more complex. Analysis of the signal evolution shows that there are at least two processes proceeding on different time scales. A signal with a broad absorption band with a maximum at approximately 470 nm and a band below 280 nm (Fig. 7A) exhibit a rapid exponential decay (Fig. 7C) with a rate constant of 1.0×10^6 s^{-1}. As this signal is readily quenched by oxygen, it was attributed to KNY triplet state. To check this assignment, we performed acetone-sensitized photolysis of KNY using 1.2 M acetone (Ac) and 4.1×10^{-4} M KNY aqueous solution (pH 6.9) upon 308 nm excitation with a XeCl laser:

$$\mathrm{Ac} \xrightarrow{h\nu} {}^{\mathrm{T}}\mathrm{Ac} + \mathrm{KNY} \rightarrow \mathrm{Ac} + {}^{\mathrm{T}}\mathrm{KNY} \qquad (1)$$

The resulting spectrum (not shown) is very similar to that obtained in the direct photolysis (Fig. 7A, triangles), confirming that the intermediate observed in the direct photolysis is indeed the triplet state of KNY. The absorption spectrum of this intermediate after correction for the bleaching of the KNY ground state is presented in Fig. 7D.

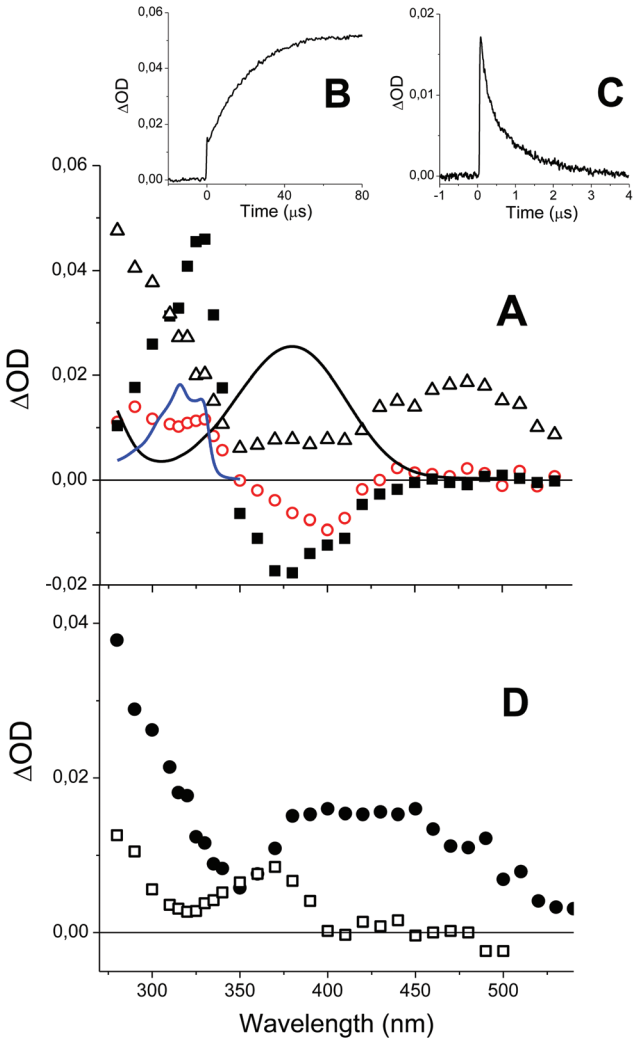

Fig. 7 TA data obtained with 2.4×10^{-4} M KNY in buffered aqueous solution, pH 7.2, under argon. (A): TA spectra recorded after 150 ns (open triangles), 1.6 μs (red circles) and 80 μs (solid squares) after 355 nm excitation. The smooth traces are the steady-state absorption spectra of KNY (black line) and 4HQN (blue line). (B) and (C): TA time profiles recorded at 330 and 430 nm, respectively. (D): Absorption spectra of KNY triplet state (solid circles) and enol form (open squares).

The other process observed in KNY photolysis manifests itself as an exponential signal growth with the rate constant of 4.7×10^4 s^{-1} in the 300–340 nm region. Fig. 7A shows the transient absorption spectra obtained 1.6 μs after the laser flash (*i.e.* at a time when the triplet decay is already completed) and 80 μs after the laser flash, and Fig. 7B shows the kinetic curve recorded at 330 nm. The spectrum at 80 μs has a maximum near 330 nm, which is very similar to the absorption spectrum of 4HQN (blue line in Fig. 7A). Since 4HQN is the major product of KNY photolysis (see above), the final product observed in flash photolysis of KNY was attributed to 4HQN. The presence of oxygen changes neither the transient spectra nor the kinetics observed after triplet decay, testifying that triplet state is not the precursor in the formation of 4HQN. The spectrum of the intermediate, which is the precursor of 4HQN, can be derived from the transient absorption spectrum at 1.6 μs after correcting for the starting compound depletion (KNY spectrum is shown in Fig. 7A, black line) and for the minor amount of 4HQN formed at 1.6 μs. The spectrum obtained is presented in Fig. 7D with open squares. This intermediate was tentatively attributed to the enol form of KNY, although we do not have solid evidence for this assignment.

The rate constants of 4HQN formation in the temperature range 300–340 K were determined from the absorption growth at 330 nm (Fig. 7B), and the following Arrhenius parameters $A = 6.8 \times 10^9$ s^{-1} and $E_a = 30$ kJ mol^{-1} were extracted from the Arrhenius plot (ESI, Fig. S6†).

The triplet quantum yields upon KNA photolysis were measured according to the procedure described earlier.[35] Briefly, the triplet quantum yields were determined by comparing the triplet state concentrations upon direct and acetone-sensitized photolysis. As an example, Fig. 8A shows transient absorption kinetics observed at 600 nm in 308 nm photolysis of KNA (1.7×10^{-4} M) in the absence (red line) and in the presence (blue line) of 1.7 M acetone (Ac). The concentrations of KNA and Ac were selected in such a way that their optical densities at 308 nm were equal: $OD_{KYN} = OD_{Ac} = 0.68$. The signal observed immediately after the laser flash is attributed to the triplet state populated in the direct KNA photolysis, while the signal growth during the first 2 μs corresponds to triplet energy transfer from ^{T}Ac to KNA. The kinetic curves were treated as a sum of exponentials:

$$\Delta OD = A \times \exp(-k_1 t) + B \times (\exp(-k_1 t) - \exp(-k_2 t)) \quad (2)$$

Here A corresponds to the intensity of the triplet signal formed in the direct photolysis, and B – to the signal from the acetone-sensitized triplet state of KNA. Eqn (2) holds as long as the pseudo-first-order triplet energy transfer reaction is much faster than the second-order triplet annihilation reaction, and the efficiency of triplet KNA formation in the acetone-sensitized photolysis is close to 100%.[35] The laser pulse energy dependence of the A and B parameters shown in Fig. 8B exhibits a deviation from linear dependence which takes place at laser intensities above 0.5 mJ per pulse. From the linear part of the plot (inset of Fig. 8B), a KNA triplet quantum yield $\Phi_T = A/B = 0.82$ can be calculated.

Similar measurements were also performed with KNY. However, due to the fast decay of triplet KNY (see Figure 7C), the rate of the signal decay in the acetone-sensitized photolysis was comparable with the rate of the signal growth and, therefore, the comparison of the signal intensities in direct and sensitized photolysis is rather inaccurate. Consequently, we are only able to make a very rough estimate of the triplet quantum yield Φ_T for direct KNY photolysis in the range 0.01–0.05.

The values obtained for the fluorescence lifetime (τ_F) and quantum yields of fluorescence, triplet and enol formations (Φ_F, Φ_T and Φ_{enol}) were used to estimate the corresponding rate constants of fluorescence, intersystem crossing (ISC), internal conversion (IC) and tautomerization (k_F, k_{ISC}, k_{IC} and k_{enol}) for both KNA and KNY in neutral aqueous solution. Since only rough estimation for Φ_T and Φ_{enol} values in KNY

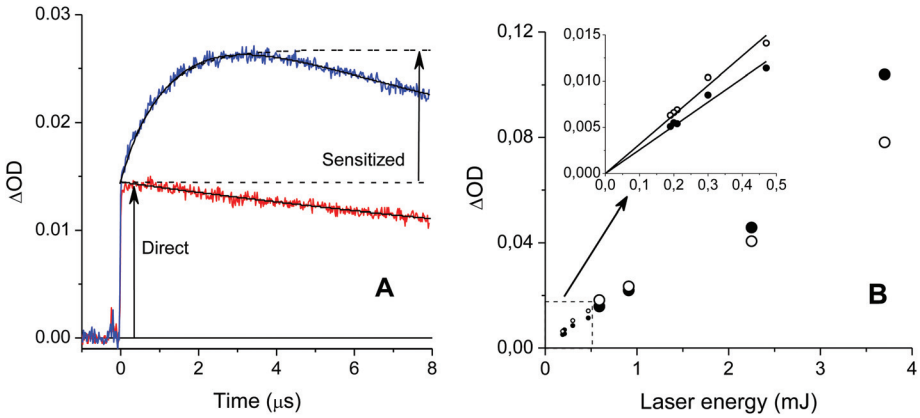

Fig. 8 (A): TA time profiles recorded at 600 nm after 308 nm excitation of neutral aqueous solution of 1.7×10^{-4} M KNA in the absence (red trace) and presence (blue trace) of 1.7 M Ac. Solid black traces: best mono- and bi-exponential fits. (B): Laser pulse energy dependence of the triplet signal generated in direct (solid circles, parameter *A* in eqn (2)) and acetone-sensitized photolysis (open circles, parameter *B* in eqn (2)) of KNA.

photolysis can be extracted from LFP data, we assumed that the yields of triplet and enol formation are equal to the yields of their decomposition products: $\Phi_T(\text{KNY}) = \Phi_{\text{DHQN}}$, $\Phi_{\text{enol}}(\text{KNY}) = \Phi_{\text{4HQN}}$ (see the Steady-state photolysis section). The calculated values are listed in Table 2. It has also been assumed that the quantum yield of internal conversion is $\Phi_{IC} = 1 - \Phi_F - \Phi_T - \Phi_{\text{enol}}$.

Discussion

Photochemistry of KNA

The photochemical properties of KNA are similar to those of the related compound 4HQN, whose photochemistry has been recently reported.[16] The major difference between 4HQN and KNA is the lower k_{IC} value for the latter, which results in a significantly higher triplet quantum yield (0.35 for 4HQN and 0.82 for KNA, see Table 2). The signal evolution observed in nanosecond flash photolysis upon UV irradiation of KNA can be described with a simple reaction scheme:

$$\text{KNA} \xrightarrow{h\nu} {}^{S1}\text{KNA} \rightarrow {}^{T}\text{KNA} \rightarrow {}^{S0}\text{KNA} \qquad (3)$$

The triplet state is the only short-lived intermediate formed in the KNA photolysis. It is characterized by an intense and narrow absorption band with peaking at 600 nm. Even at the lowest laser energies (about 2 mJ per pulse), the main channel of the triplet decay remains triplet annihilation with $k_{T-T}/\varepsilon_T \approx 5 \times 10^5$ s^{-1} cm, where k_{T-T} is the rate constant of the triplet annihilation, and ε_T is the triplet absorption coefficient at 600 nm. The contribution of the first-order decay in all measurements was below 10^4 s^{-1}. That indicates that the intrinsic triplet lifetime exceeds 100 μs.

Photophysics and photochemistry of KNY

As the photochemistry of KNY is more complex than that of KNA, it has been studied in more detail. The early excited-state dynamics of KNY is similar to that of KN.[1] It has been shown that excitation of KN and other UV filters results in a charge transfer from the amino to the carbonyl group;[35] very likely that the same charge transfer occurs during the KNY excitation, which is supported by a large Stokes shift of the fluorescence band relative to the absorption spectrum (Fig. 1). The time-dependent Stokes shift observed in Fig. 4 and 5 reflects mainly solvent relaxation around the excited KNY molecule. The first time constant τ_1 can be associated with the diffusive motion of water molecules that is known to occur with a characteristic time of about 1 ps. The second time constant might be assigned to the conformational relaxation of KNY in the excited state. The τ_2 value is two times smaller than that for KN that is most probably due to a more rigid molecular structure of KNY as compared to KN.

The excited singlet lifetime of KNY (τ_4 in Table 1) does practically not depend on the pH of the solution, but its value increases by more than a factor of two in deuterated water. That indicates that the hydrogen bonding between photoexcited KNY and solvent molecules plays a crucial role in S_1 state deactivation. Most likely, the IC mechanism of KNY is similar to that of KN and other UV filters, and includes transformation of the absorbed light energy into heat *via* hydrogen bond vibrations.[1,2,35]

Photolysis of KNY in aqueous solution results in the formation of two intermediates, observed by nanosecond flash-photolysis, namely the KNY triplet state and the species which was attributed to the KNY enol form in the ground state, and of two products detected in the irradiated samples by HPLC, *i.e.* 4HQN and DHQN. LFP data reveal unambiguously that 4HQN is the product of the thermal decomposition of the intermediate attributed to enol: the formation of 4HQN proceeds with the same rate as the enol decay, and this process is not affected by the presence of oxygen in solution.

The electronic absorption spectrum of DHQN in the 300–400 nm region practically coincides with that of KNY (inset of Fig. 3), so LFP data alone do not allow a determination of the major pathway of KNY triplet decay: it may proceed either *via* IC with the restoration of the starting compound in the ground state, or *via* chemical reaction with the

Table 2 Fluorescence lifetime (τ_F), quantum yields of fluorescence (Φ_F), triplet state (Φ_T), internal conversion (IC, Φ_{IC}), tautomerization (Φ_{enol}), anaerobic and aerobic photodecomposition (Φ_{dec}^{anaer} and Φ_{dec}^{aer}), rate constants of fluorescence (k_F), intersystem crossing (ISC, k_{ISC}), IC (k_{IC}) and tautomerization (k_{enol}) for KN, KNA, KNY, 4HQN and XAN in neutral aqueous solutions

	τ_F, ps	Φ_F	Φ_T	Φ_{IC}	Φ_{enol}	k_F, s^{-1}	k_{ISC}, s^{-1}	k_{IC}, s^{-1}	k_{enol}, s^{-1}	Φ_{dec}^{anaer}	Φ_{dec}^{aer}
KN[a]	26.9 ± 0.8	$(9.2 \pm 1.0) \times 10^{-4}$	$(7.0 \pm 1.7) \times 10^{-3}$	0.99	ND[d]	3.4×10^7	2.6×10^8	3.7×10^{10}	NM[e]	$(1.5 \pm 0.2) \times 10^{-5}$	$(3.8 \pm 0.4) \times 10^{-5}$
KNA	150 ± 30	$(1.4 \pm 0.2) \times 10^{-3}$	0.82 ± 0.15	0.17	ND	9.1×10^7	5.5×10^9	1.1×10^9	NM	$(6.0 \pm 1.5) \times 10^{-3}$	$(2.6 \pm 0.6) \times 10^{-3}$
KNY	370 ± 30	$(7.5 \pm 1.0) \times 10^{-3}$	$(2.2 \pm 0.6) \times 10^{-2}$	0.96	$(1.2 \pm 0.4) \times 10^{-2}$	2.0×10^7	5.9×10^7	2.6×10^9	3.2×10^7	$(3.0 \pm 0.8) \times 10^{-2}$	$(8 \pm 2) \times 10^{-3}$
4HQN[b]	110 ± 11	$(1.1 \pm 0.1) \times 10^{-2}$	0.35 ± 0.07	0.64	ND	1.0×10^8	3.2×10^9	5.8×10^9	NM	NM	NM
XAN[c]	11 ± 1	$(1.0 \pm 0.1) \times 10^{-3}$	ND	NM	≈1	9.1×10^7	NM	NM	9.1×10^{10}	$<10^{-5}$	$(8.2 \pm 1.8) \times 10^{-5}$

[a] From ref. 35. [b] From ref. 16. [c] From ref. 17. [d] ND – not detected. [e] NM – not measured.

formation of DHQN. However, the results obtained in the steady-state photolysis give strong evidence in favor of the second pathway: DHQN formation occurs efficiently under anaerobic conditions only, and quenching of the KNY triplet state by oxygen blocks this process. The yield of DHQN formation is similar to the KNY triplet yield, which is an additional confirmation that DHQN is a direct product of triplet KNY scission. To further confirm this conclusion, we performed acetone-sensitized photolysis of KNY in aqueous solution. A sample containing 3.4×10^{-4} M of KNY and 1.4 M of acetone at pH 7.2 was irradiated with 0.5 mJ XeCl laser pulses at 308 nm. Aliquots of 15 μl were taken periodically, the concentrations of KNY and DHQN were measured by HPLC, and the yields of KNY decomposition and product formation were calculated from the dependences of the concentrations on the number of light quanta absorbed by the sample (ESI, Fig. S7†). Under such conditions, both KNY decomposition and DHQN formation quantum yields (0.30 and 0.26, respectively) were approximately 10-fold greater than upon direct photolysis. This finding confirms that the KNY triplet state is the direct precursor of DHQN.

The results obtained provide a complete picture of the processes taking place upon UV irradiation of aqueous solution of KNY (Scheme 1). Photoexcitation results in the population of the Frank–Condon (vibrationally, solvent and conformationally unrelaxed) S_1 excited state; all relaxations proceed on the picosecond time scale. According to the results obtained, the major pathways of the relaxed S_1 state decay are internal conversion, intersystem crossing, fluorescence and tautomerization into the enol form, proceeding with the rate constants k_{IC}, k_{ISC}, k_F and k_{enol} (Table 2). The most important channel of the S_1 state decay is IC, leading to the restoration of the starting compound in the ground state and proceeding with a quantum yield of $\Phi_{IC} \approx 0.96$ and a rate constant of $k_{IC} = 2.6 \times 10^9$ s^{-1}. The other channels, namely fluorescence ($\Phi_F = 0.0075$, $k_F = 2.0 \times 10^7$ s^{-1}), intersystem crossing to the triplet state ($\Phi_T = 0.022$, $k_{ISC} = 5.9 \times 10^7$ s^{-1}), and tautomerization into the enol form ($\Phi_{enol} = 0.012$, $k_{enol} = 3.2 \times 10^7$ s^{-1}) contribute significantly less to the overall decay of the S_1 excited state population. The major decay channel of KNY triplet state is decarboxylation ($k = 1.0 \times 10^6$ s^{-1}) yielding DHQN, whereas thermal decarboxylation of the enol ($A = 6.8 \times 10^9$ s^{-1}, $E_a = 30$ kJ mol^{-1}, $k_{(300\ K)} = 4.7 \times 10^4$ s^{-1}) results in the formation of 4HQN.

Table 2 summarizes the major photochemical properties of KN and its decomposition products, KNA and KNY, studied in the present work, and 4HQN and XAN, whose photochemical properties have been reported earlier.[16,17] It demonstrates that all the decomposition products are better photosensitizers than KN itself. KNA, KNY and 4HQN have significantly longer singlet excited-state lifetimes and much higher triplet and photodecomposition yields. This difference originates from specific mechanisms of IC for KN and other UV filters. Excitation of KN results in an increase of the electron density on the carbonyl oxygen that augments the acidity of the amino group and the basicity of the carbonyl group, which, in turn,

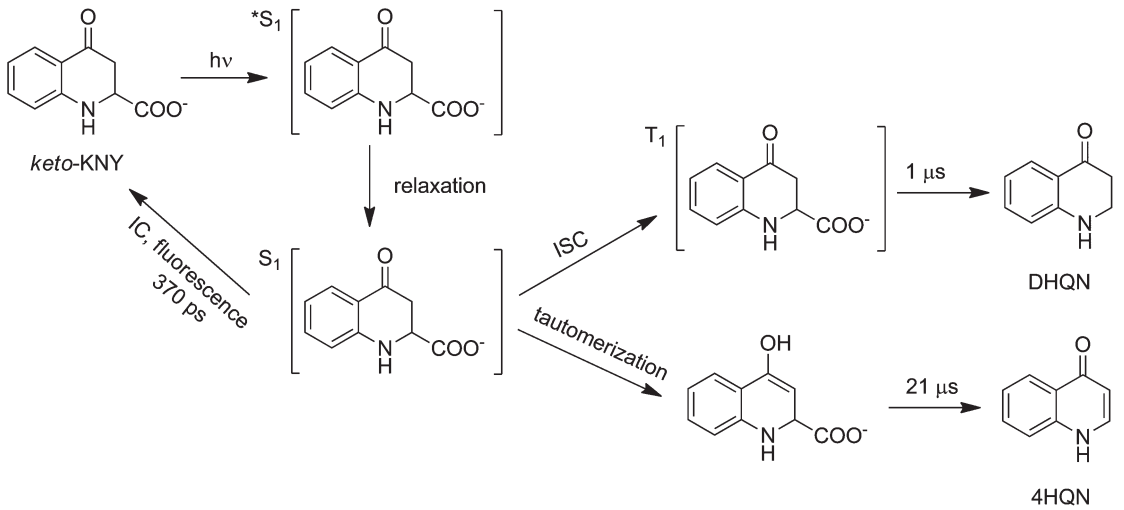

Scheme 1

leads to an enhancement of their hydrogen bonding ability. The stretching vibrations of the hydrogen bonds act as accepting modes for the $S_1 \rightarrow S_0$ non-radiative transition and thus the electronic energy dissipates through the hydrogen bonds as vibrational energy.[1] As a result, solvent-assisted IC, based on the hydrogen bonding interactions between KN in the S_1 state and the solvent molecules, proceeds very fast, and becomes the main deactivation channel of the S_1 state in protic solvents. In KNY, this mechanism is apparently less effective. In the case of KNA and 4HQN, the absence of isotope effects points to an insignificant role of solvent-assisted IC in the decay of S_1 state population. This should be explained by aromatic conjugation, which reduces the charge transfer from nitrogen to the carbonyl group after the optical excitation. This is supported by the markedly smaller fluorescence Stokes shifts of KNA as compared with KNY ($\Delta\nu = 3.8 \times 10^3$ cm^{-1} for KNA and $\Delta\nu = 7.1 \times 10^3$ cm^{-1} for KNY, Fig. 1). The absorption spectrum of KNY is red-shifted compared to KNA (Fig. 1), although KNA has a more extended conjugated system; this observation may also be attributed to a stronger charge transfer upon excitation in the case of KNY. On the other hand, the inclusion of a nitrogen atom into an aromatic system enhances the spin–orbit coupling and accelerates ISC.[38–41] In total, the values of k_{IC} for these compounds are by order of magnitude lower than for KN, and the ISC to the triplet state plays an important role in the S_1 state decay, especially for KNA and 4HQN.

XAN is an exception among the decomposition products of KN: its singlet excited-state lifetime in aqueous solution is even shorter than that for KN (Table 2), the population of the triplet state has not been detected,[17] and the photostability under anaerobic conditions is very high. However, the decay of the XAN singlet excited state occurs with the formation of an enol form, the latter converting back into the starting keto form on the nanosecond time scale (both enol and keto forms are in the ground state).[17] The enol form of XAN might be significantly more reactive than the keto form, and may cause damages to the surrounding molecules. Indeed, enhanced oxidation and polymerization of lens proteins upon their UV irradiation in the presence of XAN have been reported.[42,43] The photochemical formation of the enol form has been also detected in the photolysis of KNY aqueous solutions in the present work. Although the rate constant and the quantum yield of enol formation are much lower for KNY than for XAN (Table 2), the enol form of KNY seems to be significantly more reactive than that of XAN: the decay of the XAN enol results in the restoration of the keto form, whereas KNY enol undergoes decarboxylation yielding 4HQN. The instability of the triplet state and the enol form of KNY is the main factor behind the low photochemical stability of this compound, and, probably, the main reason why KNY has never been detected in the human or animal's lens. Most likely, the rate of KNY formation inside the lens is much lower than its decomposition rate, so the steady-state concentration of KNY is extremely low.

Conclusions

The cyclization of KN results in the formation of products, which, under UV irradiation, generate significantly larger amounts of reactive species as compared with the parent KN. In the case of KNY with an unconjugated cycle, two species, *i.e.* the triplet state and the species attributed to the enol form, are generated with relatively small yields of $\Phi_T \approx 2\%$ and $\Phi_{enol} \approx 1\%$. These intermediates are unstable and are rapidly transformed into subsequent products, DHQN and 4HQN, from the triplet state and the enol form, respectively. In the case of KNA, with a conjugated cycle, the only reactive species is the triplet state, which is populated with a tremendously high yield, around 80%. The observed short-lived species and their products might react with the protein environment of the lens and might contribute to the development of oxidative stress conditions, the main factor of the development of cataract.

Acknowledgements

This work was supported by RFBR (Projects 11-04-00143, 11-03-00296 and 12-04-31244), by the Division of Chemistry of RAS, by the Government of the Russian Federation (grants 11. G34.31.0045 and 2012-1.2.1-12-000-1013-009), by the President of the Russian Federation (grant NSh-2429.2012.3), by the Presidium of Russian Academy of Science (N 21.13), and by Fonds National Suisse de la Recherche Scientifique (project no. 200020-124393).

References

1 P. S. Sherin, J. Grilj, Yu. P. Tsentalovich and E. Vauthey, Ultrafast excited-state dynamics of kynurenine – a UV filter of the human eye, *J. Phys. Chem. B*, 2009, **113**, 4953.
2 P. S. Sherin, J. Grilj, L. V. Kopylova, V. V. Yanshole, Yu. P. Tsentalovich and E. Vauthey, Photophysics and photochemistry of UV filter kynurenine covalently attached to amino acids and to a model protein, *J. Phys. Chem. B*, 2010, **114**, 11909.
3 R. van Heyningen, Fluorescent glucoside in the human lens, *Nature*, 1971, **230**, 393.
4 A. M. Wood and R. J. W. Truscott, UV filters in human lenses: tryptophan catabolism, *Exp. Eye Res.*, 1993, **56**, 317.
5 A. M. Wood and R. J. W. Truscott, Ultraviolet filter compounds in human lenses: 3-hydroxykynurenine glucoside formation, *Vision Res.*, 1994, **34**, 1369.
6 F. Moroni, Tryptophan metabolism and brain function: focus on kynurenine and other indole metabolites, *Eur. J. Pharmacol.*, 1999, **375**, 87.
7 L. M. Taylor, J. A. Aquilina, J. F. Jamie and R. J. W. Truscott, UV filter instability: consequences for the human lens, *Exp. Eye Res.*, 2002, **75**, 165.
8 Yu. P. Tsentalovich, O. A. Snytnikova, M. D. E. Forbes, E. I. Chernyak and S. V. Morozov, Photochemical and thermal reactivity of kynurenine, *Exp. Eye Res.*, 2006, **83**, 1439.
9 L. M. Taylor, J. A. Aquilina, J. F. Jamie and R. J. W. Truscott, Glutathione and NADH, but not ascorbate, protect lens proteins from modification by UV filters, *Exp. Eye Res.*, 2002, **74**, 503.
10 L. V. Kopylova, O. A. Snytnikova, E. I. Chernyak, S. V. Morozov and Yu. P. Tsentalovich, UV filter decomposition. A study of reactions 4-(2-aminophenyl)-4-oxocrotonic acid with amino acids and antioxidants present in the human lens, *Exp. Eye Res.*, 2007, **85**, 242.
11 L. M. Bova, M. H. J. Sweeney, J. F. Jamie and R. J. W. Truscott, Major changes in human ocular UV protection with age, *Invest. Ophthalmol. Vis. Sci.*, 2001, **42**, 200.
12 H. Z. Malina and X. D. Martin, Xanthurenic acid derivative formation in the lens is responsible for senile cataract in humans, *Graefe's Arch. Clin. Exp. Ophthalmol.*, 1995, **233**, 38.
13 H. Z. Malina and X. D. Martin, Deamination of 3-hydroxykynurenine in bovine lenses: a possible mechanism of cataract formation in general, *Graefe's Arch. Clin. Exp. Ophthalmol.*, 1996, **234**, 723.
14 B. K. Zsizsik and R. Hardeland, Formation of kynurenic acid and xanthurenic acid from kynurenine and 3-hydroxykynurenine in the dinoflagellatae Lingulodinum polyedrum: role of a novel, oxidative pathway, *Comp. Biochem. Physiol., Part C: Toxicol. Pharmacol.*, 2002, **133**, 383.
15 T. Zarnowski, R. Rejdak, Z. Zagorski, A. G. M. Juenemann, E. Zrenner, T. Kocki, E. M. Urbanska and W. A. Turski, Content of kynurenic acid and activity of kynurenine aminotransferases in mammalian eyes, *Ophthalmic Res.*, 2004, **36**, 124.
16 P. S. Sherin, N. P. Gritsan and Yu. P. Tsentalovich, Experimental and quantum chemical study of photochemical properties of 4-hydroxyquinoline, *Photochem. Photobiol. Sci.*, 2009, **8**, 1550.
17 V. V. Yanshole, P. S. Sherin, N. P. Gritsan, O. A. Snytnikova, V. I. Mamatyuk, J. Grilj, E. Vauthey, R. Z. Sagdeev and Y. P. Tsentalovich, Photoinduced tautomeric transformations of xanthurenic acid, *Phys. Chem. Chem. Phys.*, 2010, **12**, 9502.
18 J. Mizdrak, P. G. Hains, R. J. W. Truscott, J. F. Jamie and M. J. Davies, Tryptophan-derived ultraviolet filter compounds covalently bound to lens proteins are photosensitizers of oxidative damage, *Free Radical Biol. Med.*, 2008, **44**, 1108.
19 E. Okuno, F. Du, T. Ishikawa, M. Tsujimoto, M. Nakamura, R. Schwarcz and R. Kido, Purification and characterization of kynurenine-pyruvate aminotransferasefrom rat kidney and brain, *Brain Res.*, 1990, **534**, 37.
20 R. Rejdak, T. Zarnowski, W. A. Turski, E. Okuno, T. Kocki, Z. Zagórski, K. Kohler, E. Guenther and E. Zrenner, Presence of kynurenic acid and kynurenine aminotransferases in the inner retina, *NeuroReport*, 2001, **12**, 3675.
21 W. A. Turski, M. Nakamura, W. P. Todd, B. K. Carpenter, W. O. Whetsell and R. Schwarcz, Identification and quantification of kynurenic acid in human brain tissue, *Brain Res.*, 1988, **454**, 164.
22 P. Milart, E. M. Urbanska, W. A. Turski, T. Paszkowski and R. Sikorski, Kynurenine aminotransferase I activity in human placenta, *Placenta*, 2001, **22**, 259.
23 T. Zarnowski, R. Rejdak, E. Zielinska-Rzecka, E. Zrenner, P. Grieb, Z. Zagórski, A. Junemann and W. A. Turski, Elevated concentrations of kynurenic acid, a tryptophan derivative, in dense nuclear cataracts, *Curr. Eye Res.*, 2007, **32**, 27.
24 V. R. Kanth, K. Lavanya and J. Srinivas, Elevated expression of indoleamine 2,3-dioxygenase (IDO) and accumulation of kynurenic acid in the pathogenesis of STZ-induced diabetic cataract in wistar rats, *Curr. Eye Res.*, 2009, **34**, 274.
25 M. P. Pileni, M. Giraud and R. Santus, Kynurenic acid. I. Spectroscopic properties, *Photochem. Photobiol.*, 1979, **30**, 251.
26 M. P. Pileni, M. Giraud and R. Santus, Kynurenic acid. II. Photosensitizing properties, *Photochem. Photobiol.*, 1979, **30**, 257.

27 C. M. Krishna, S. Uppuluri, P. Riesz, J. S. Zigler Jr. and D. Balasubramanian, A study of the photodynamic efficiencies of some eye lens constituents, *Photochem. Photobiol.*, 1991, **54**, 51.

28 R. Lugo-Huitrón, T. Blanco-Ayala, P. Ugalde-Muñiz, P. Carrillo-Mora, J. Pedraza-Chaverrí, D. Silva-Adaya, P. D. Maldonado, I. Torres, E. Pinzón, E. Ortiz-Islas, T. López, E. García, B. Pineda, M. Torres-Ramos, A. Santamaría and V. Pezez-De La Cruz, On the antioxidant properties of kynurenic acid: free radical scavenging activity and inhibition of oxidative stress, *Neurotoxicol. Teratol.*, 2011, **33**, 538.

29 R. Rusakowicz and A. C. Testa, 2-Aminopyridine as a standard for low-wavelength spectrofluorimetry, *J. Phys. Chem.*, 1968, **72**, 2680.

30 B. Gelernt, A. Findeisen, A. Stein and J. A. Poole, Absolute measurement of the quantum yield of quinine bisulphate, *J. Chem. Soc., Faraday Trans. 2*, 1974, **70**, 939.

31 J. R. Calvert and J. N. Pitts, *Photochemistry*, John Willey, New-York, 1969.

32 (*a*) A. Morandeira, L. Engeli and E. Vauthey, Ultrafast charge recombination of photogenerated ion pairs to an electronic excited state, *J. Phys. Chem. A*, 2002, **106**, 4833; (*b*) G. Duvanel, J. Grilj, H. Chaumeil, P. Jacques and E. Vauthey, Ultrafast excited-state dynamics of a series of zwitterionic pyridinium phenoxides with increasing sterical hindering, *Photochem. Photobiol. Sci.*, 2010, **9**, 908–915.

33 G. Duvanel, N. Banerji and E. Vauthey, Excited-state dynamics of donoracceptor bridged systems containing a boron-dipyrromethene chromophore: interplay between charge separation and reorientational motion, *J. Phys. Chem. A*, 2007, **111**, 5361.

34 N. Banerji, G. Duvanel, A. Perez-Velasco, S. Maity, N. Sakai, S. Matile and E. Vauthey, Excited-state dynamics of hybrid multichromophoric systems: toward an excitation wavelength control of the charge separation pathways, *J. Phys. Chem. A*, 2009, **113**, 8202.

35 Yu. P. Tsentalovich, P. S. Sherin, L. V. Kopylova, I. V. Cherepanov, J. Grilj and E. Vauthey, Photochemical properties of UV filter molecules of the human eye, *Invest. Ophthalmol. Visual Sci.*, 2011, **52**, 7687.

36 Yu. P. Tsentalovich, O. A. Snytnikova, P. S. Sherin and M. D. E. Forbes, Photochemistry of kynurenine, a tryptophan metabolite: properties of the triplet state, *J. Phys. Chem. A*, 2005, **109**, 3565.

37 (*a*) S. F. Mason, The tautomerism of N-heteroaromatic hydroxycompounds. Part I. Infrared spectra, *J. Chem. Soc.*, 1957, 4874; (*b*) S. F. Mason, The tautomerism of *N*-heteroaromatic hydroxycompounds. Part II. Ultraviolet spectra, *J. Chem. Soc.*, 1957, 5010; (*c*) S. F. Mason, The tautomerism of N-heteroaromatic hydroxycompounds. Part III. Ionization constants, *J. Chem. Soc.*, 1958, 674.

38 S. K. Lower and M. A. El-Sayed, The triplet state and molecular electronic processes in organic molecules, *Chem. Rev.*, 1966, **66**, 199.

39 M. A. El-Sayed and R. G. Brewer, Polarization of the $\pi \rightarrow \pi$ and $\pi \rightarrow$ n phosphorescence spectra of *N*-heterocyclics, *J. Chem. Phys.*, 1963, **39**, 1623.

40 E. C. Lim and J. M. H. Yu, Vibronic interaction between (n, π) and (π, π) states and spin—orbit coupling in nitrogen heterocyclic, *J. Chem. Phys.*, 1966, **45**, 4742.

41 K. Schmidt, S. Brovelli, V. Coropceanu, D. Beljonne, J. Cornil, C. Bazzini, T. Caronna, R. Tubino, F. Meinardi, Z. Shuai and J. L. Brédas, Intersystem crossing processes in nonplanar aromatic heterocyclic molecules, *J. Phys. Chem. A*, 2007, **111**, 10490.

42 H. Z. Malina, Xanthurenic acid provokes formation of unfolded proteins in endoplasmic reticulum of the lens epithelial cells, *Biochem. Biophys. Res. Commun.*, 1999, **265**, 600.

43 J. E. Roberts, E. L. Finley, S. A. Patat and K. L. Schey, Photooxidation of lens protein with xanthurenic acid: a putative chromophore for cataractogenesis, *Photochem. Photobiol.*, 2001, **74**, 740.

